Hundalee Fault, North Canterbury, New Zealand: Late Quaternary activity and regional tectonics

David J.A. Barrell[a]*, Mark W. Stirling[b], Jack N. Williams[b], Katrina M. Sauer[b,c], Ella J. van den Berg[d]

[a]GNS Science, Dunedin, New Zealand; [b]University of Otago, Dunedin, New Zealand; [c]US Geological Survey, Denver, CO, USA; [d]Pattle Delamore Partners Ltd, Auckland, New Zealand

Supplementary Information

This Supplement begins with a review and assessment of information on the Holocene and Pleistocene terraces along the Conway section of the North Canterbury coast (Sections S1 and S2). The purpose is to assess whether previous estimates of coastal uplift rates, some dating back to the mid-1980s, especially Ota et al. (1984), still remain appropriate in light of more recent information. This is followed by description and assessment of the Okarahia valley fluvial terrace sequence (Section S3). Section S4 describes structural modelling, Section S5 discusses Kaikōura Peninsula marine terraces and structural interpretation, and Section S6 discusses aftershock distributions.

Section S1: Conway Flat Holocene coastal terraces

Lidar reveals much morphological detail of the Conway Flat terraces (location in Figure 1 of main text). North of Conway River, the Conway Flat 1 (CF1) terrace has a broad seaward crest at ~14–15 m a.s.l. that slopes gently inland to a trough at the foot of the coastal cliff at the back of the Holocene terraces (Figures S1, S2; P1-P2). Seaward of CF1 is a succession of closely spaced beach ridge crests of approximately even height at ~11–12 m a.s.l (CF2 terrace surface). Farther seaward is a narrow terrace remnant (CF3) with beach ridge crests at ~6–7 m a.s.l. The modern beach ridge crests stand between ~4 and ~6 m a.s.l. depending on location, being lower on the active beach bar across the Conway River mouth and higher where accumulated against older terraces.

South of Conway River is a broad-crested terrace standing ~12–13 m a.s.l., with a gentle slope landward to a broad plain standing ~8–9 m a.s.l (P3, Figures S1, S2). We interpret these features as a constructional barrier landform (beach complex) with a landward ‘lagoon plain’, both part of the CF1 terrace unit. This differs from the Ota et al. (1984) interpretation of the lower landward plain as CF1, and the seaward higher broad terrace as CF2. Our CF1 interpretation seems more compatible with the broad landward slope of the ‘beach complex’ landform both sides of the Conway River (Figure S2; P1-P3). At the landward margin of the Conway Flat terraces is a substantial cliff, several tens of metres high, which by its setting and sharpness of form is of post-glacial age.

Southwest from the Conway River mouth, the terrace sequence is progressively cut out along the active coastal cliff (Figure S1). About 5 km south of the river mouth, the active cliff transects the boundary between the older post-glacial cliff and the ‘lagoon plain’ sector of the CF1 terrace. Exposed sediments of the CF1 terrace, as described by Ota et al. (1984), are predominantly silt with some buried trees in growth position. The trees attest to an episode of land surface stability and vegetation growth followed by a sediment aggradation episode that buried the vegetation. Radiocarbon dating of three buried trees returned calendar ages of 8.4 ± 0.2 ka (A-3), 9.2 ± 0.5 ka (B-3) and 8.6 ±0.2 ka (578) (Figure S1; Table S1). The trees are in about the same stratigraphic position and it is unclear why one has a median age ~700 years older than the other two trees. However, the age ranges intersect at ~8.6—~8.7 ka, so we adopt 8.6 ka as the time of onset of forest burial, just prior to the boundary (8.2 ka) between the

Early and Middle Holocene time intervals (Gibbard and Head 2020). The buried trees are at the foot of the older post-glacial sea cliff and afford a minimum age for the cliff, which means the cliff is of Early Holocene age (Figures S1, S2).

As explained by Clement et al. (2016), global glacioisotasy effects meant that, inter-regionally, culminations of post-glacial sea rise were not synchronous and maximum levels attained not uniform. New Zealand's longest paleoenvironmental dataset for Holocene sea rise is at Christchurch (*op. cit.*). At ~9 ka, the sea was rising at ~0.8 m per century until culmination at ~7 ka. Christchurch sea level at ~8.6 ka was between about -15 and -7 m a.s.l. In the southwestern North Island, sea rise had culminated by ~7.5 ka. In contrast, glacial-isostatic adjustment (GIA) models indicate that sea rise in New Zealand should have culminated at ~8 ka (Clement et al. 2016). No specific data exist for Holocene sea level on the Conway coast.

Given these issues, we employ simplifying assumptions for our uplift assessment. First, we assume that the post ~9 ka sea rise was progressive, without stillstands or reversals. Second, we assume that the sea rise culminated at ~0 m a.s.l. and remained at about that level. These assumptions may be incorrect but enable a first-approximation assessment of Holocene uplift without encumberment from various ill-constrained uncertainties.

Of particular geomorphologic relevance is that (1) the now-buried trees grew seaward of the Early Holocene sea cliff, and (2) at the time the trees grew, the post-glacial sea rise was still in progress. An area seaward of the Early Holocene cliff became land due to a relative sea level fall prior to ~8.6 ka, which we infer was an uplift event or events. To allow sufficient time for woody vegetation to colonise the former shore platform, we assume that the uplift occurred at least a century prior to ~8.6 ka. The sea at that time was rising ~0.8 m per century, suggesting uplift of at least 2 m in order to expose the shore platform and maintain it as land while the trees grew. Ota et al. (1984) inferred that the tree-burying silt was deposited in a brackish to littoral environment based on diatom analysis. They did not report any bioturbation or intertidal shell species which could indicate fully marine conditions.

We infer that sediment aggradation ending in formation of the CF1 terrace related to the last part of post-glacial sea rise. We envision a barrier bar (beach facies) that enclosed a lagoon (lagoon facies) (Figure S2; P4 interpreted). Episodes of fan building from nearby streams provided lenses of gravel that Ota et al. (1984) show within the silt unit. Sedimentation presumably kept pace with sea rise, otherwise the lagoonal area should have experienced marine inundation. The rising sea also provided accommodation space that allowed progressive coastal sediment aggradation.

The modern Conway coast storm beach crest at ~5 m a.s.l. (Figure S2, P2) is an analogue for the original elevation of the CF1 beach complex crest, under the assumption of post-glacial sea rise culmination at 0 m a.s.l. The landward CF1 lagoon plain stands 3 to 5 m lower, implying original elevation of between 0 to 2 m a.s.l, which seems reasonable for a barrier-enclosed environment. The present elevations of the CF1 beach complex (~12–13 m) and lagoon plain (~8–9 m) south of Conway River imply that ~8 m of uplift has occurred since ~8.6 ka. This indicates a Middle to Late Holocene uplift rate of ~1.1 mm/yr, a minimum value because ~8.6 ka is a maximum age for the CF1 terrace surface. However, the buried trees provide a minimum age, probably a close minimum, for stranding of the Early Holocene coastal cliff with inferred uplift of at least 2 m. Thus, a minimum of ~10 m uplift has occurred approximately since 8.6 ka, yielding a Middle to Late Holocene uplift rate of ~1.2 mm/yr. While not a maximum rate, it underscores that Middle-Late Holocene net uplift at this location has been somewhat more than 1.0 mm/yr.

In contrast, Ota et al. (1984) calculated a ~2–3 mm/yr Holocene uplift rate based on the oldest dated tree (8,400 years BP radiocarbon age; ~9.2 ka calibrated) and inferred contemporary sea level of -24 m a.s.l. That scenario carries an implication that the CF1 terrace area should have been thoroughly drowned if the sea still had ~24 m to rise at ~0.8 mm/yr. Our interpretation using a best-fit tree age of ~8.6 ka with sea level not far short of its culmination, could account for the marginal marine, rather than fully marine, character of the silt underlying CF1.

North of Conway River, the CF1 beach complex crest stands ~14–15 m a.s.l., ~2 m higher than farther south (Figure S2, P1-P3). Late Cenozoic stratigraphy indicates a northwest-striking fault under the Conway River coastal reach (Warren 1995). To the north, Paleogene strata dip southeast off basement and Greta Formation is absent. South, Paleogene strata are excised and Greta Formation dips east off basement. Although Pliocene uplift to the south is indicated, post-Early Holocene upthrow to the north offers one simple explanation for the CF1 height difference across the Conway River. North of the Conway, the CF2 terrace comprises beach ridges ~2–3 m lower than the CF1 beach complex crest, implying the CF1 terrace was uplifted by that amount prior to CF2 beach accumulation. Similarly, CF2 ridge crests stand ~4–6 m higher than those of the CF3 terrace, implying that ~5 m of uplift raised the CF2 terrace above shoreline activity. CF3 terrace beach ridge crests are ~1–2 m higher than those of the modern beach, suggesting further uplift. At least three post-8.6 ka uplift events are indicated.

Section S2: Pleistocene coastal terraces of the Conway coast

The Tarapuhi, Kemps Hill and Amuri Bluff terraces are associated with marine erosion surfaces and overlying beach or near-shore sediments, typically capped by colluvium and/or loess (Ota et al. 1984). The Claverley terrace is associated with alluvial fans that grade over the Amuri Bluff terrace unit. Warren (1995) defined formation names for the deposits of each terrace level, with the Trig T, Kemps Hill, Wenlock and Te Mania formations corresponding respectively to deposits of the Tarapuhi, Kemps Hill, Amuri Bluff and Claverley geomorphic terraces. While a valid stratigraphic approach, for simplicity we use the Ota et al. (1984, 1996) geomorphic terminology.

Deltaic sedimentary strata exposed in coastal cliffs between ~4 and ~11 km southwest of Conway River were assigned a late Quaternary age by Lewis and Ekdale (1991). They interpreted the coastal terraces as forming the upper surfaces (i.e. top-sets) of the deltaic sediment packages. Warren (1995), using biostratigraphy, considered the deltaic strata to be Pliocene-age Greta Formation (Hawkswood deltaic lithofacies) and stated as incorrect the Lewis and Ekdale (1991) age interpretation. However, some workers have persisted with the Quaternary age interpretation (McConnico and Bassett 2007; McConnico 2012). Greywacke clasts in the deltaic strata are predominantly subrounded, as seen in photographs in Warren (1995) and McConnico (2012). We think it implausible that such rounding could be achieved over fluvial transport distances of no more than 5 km from adjacent Hawkswood range-front source catchments. More likely, the deltaic sediments were sourced from larger fluvial systems, in a paleogeographic setting pre-dating the present topography and adjacent bathymetry. We adopt the Ota et al. (1984, 1996) and Warren (1995) mapping of the Conway coastal terraces comprising marine or fluvial sediment veneers unconformably overlying older sedimentary strata. We treat the late Quaternary deltaic deposition model, and associated, previously unreported, thrust faulting along the eastern side of the Hawkswood Range set out by McConnico (2012), as unconfirmed and do not use those inferences in our late Quaternary uplift interpretation.

Detailed assessment and interpretation of the Conway coastal terrace sequence by Oakley et al. (2018) involved the assignment of paleoshoreline elevations (partly modelled from assumed terrace sediment thickness values), the application of inferred ages and uncertainties of correlative sea level maxima, and resulting derivation of uplift rates and uncertainties. While acknowledging the validity of that approach, our assessment uses generalised estimates of both terrace elevation and inferred sea levels, to derive indicative uplift estimates, without explicit uncertainties. The purpose is to facilitate general geomorphological and tectonic comparisons and interpretations, rather than specifically quantified deformation rates for coastal uplift.

Ages for the Pleistocene Conway coastal terraces have commonly been estimated via correlation of terraces to interglacial sea-level maxima on the Quaternary eustatic sea level curve (e.g. Siddall et al. 2003; Creveling et al. 2017) (Figure S3), based on relative terrace elevations. Since the 1990s, this correlation method has been further informed by direct dating of terraces at Haumuri Bluffs via the relative-age estimation method of amino acid racemisation (AAR) on fossil shells and optically stimulated luminescence (OSL) dating of marine sand deposits (Ota et al. 1996; Oakley et al. 2017). The dating is sparse, with only one and three samples dated from the Amuri Bluff and Tarapuhi terraces, respectively. Two AAR ages for shells preserved in the Tarapuhi terrace marine sediments have been reported, comprising 135 $\pm$ 35 ka (Ota et al. 1996), and 60–136 ka with a preferred median of 94 ka (Oakley et al. 2017). Two OSL ages were obtained by Oakley et al. (2017) for sand samples, one from the Tarapuhi terrace (95 $\pm$ 10 ka) and one from the Amuri Bluff terrace (74 $\pm$ 9 ka).

Differing age interpretations have been offered for the Tarapuhi terrace. It was correlated with the antepenultimate interglacial (Marine Isotope Stage (MIS) 9; 300 to 337 ka, Lisiecki and Raymo 2005) by Ota et al. (1984) and Rattenbury et al. (2006), with the penultimate interglacial (MIS 7; 191 to 243 ka, Lisiecki and Raymo 2005) by Fleming and Suggate (1964) and with the Last Interglacial (MIS 5; 71 to 130 ka, Lisiecki and Raymo 2005) by Ota et al. (1996) and Oakley et al. (2017). The latter two interpretations attributed the Tarapuhi terrace to MIS 5c (second peak of Last Interglacial climate; ~100 ka; Figure S3A), the Kemps Hill terrace to either late MIS 5c or early MIS 5a, and the Amuri Bluff terrace to MIS 5a (final peak of Last Interglacial climate; ~80 ka; Figure S3A). Irrespective of the various age interpretations of the older terraces, previous workers all favour correlation of the Amuri Bluff terrace with MIS 5a, the last sea level maximum of the Last Interglacial (Figure S3). This correlation is compatible with the 74 ± 9 ka OSL age obtained by Oakley et al. (2017) for the terrace's marine sediments. It is also commensurate with overall geomorphology, with the Amuri Bluff terrace marking the last marine erosion episode of the last interglacial, followed by sustained marine regression signifying the last glaciation, and accumulation across the abandoned sea floor of alluvial fan deposits representing the Claverley terrace (Figure S3).

Tarapuhi terrace marine sediments contain a cool-water fossil shell fauna, sampled for AAR dating, whose modern faunal equivalent lives no farther north than Foveaux Strait, ~4° of latitude to the south of Haumuri Bluffs (Fleming and Suggate 1964; Ota et al. 1996). Shell faunas from the highest marine terrace on Kaikōura Peninsula have a similarly cool affinity (*op. cit.*). The presence of cool water fauna has made previous workers reluctant to correlate the Tarapuhi terrace with the peak of an interglacial episode, such as MIS 5e (120 ka), but rather to favour an interstadial age, such as MIS 5c, on the presumption that conditions were cooler than peak interglacial (Fleming and Suggate 1964; Ota et al. 1996).

A recent hypothesis that glacial-interglacial climate shifts were initiated in the Southern Hemisphere (Denton et al. 2021) offers another possibility, wherein changes in Northern Hemisphere (NH) continental ice sheet volume, and hence eustatic sea level, were controlled from the south. In that view, onset of glacial-mode conditions in the Southern Ocean, with northward shift of the Subtropical Front and incursion of cooler water around the South Island, would have preceded NH ice build-up and associated eustatic sea level fall. Thus, cool-water indicators at the culmination of an interglacial maximum may not be anomalous along the eastern South Island and need not imply less-than-peak interglacial sea level. This consideration would also remove any necessity that the apparently unusual fauna from the highest terrace at Kaikōura Peninsula and the Tarapuhi terrace means that the two terraces are very likely coeval (Ota et al. 1996).

The Marine Isotope Stage (MIS) 5c age (~100 ka) assigned to the 175 m a.s.l Tarapuhi terrace paleoshoreline at Haumuri Bluffs by Ota et al. (1996) and Oakley et al. (2017, 2018) implies that net uplift at Haumuri Bluffs was much faster prior to 80 ka than afterwards. We note, however, that the age interpretation is based on sparse dating results for the Tarapuhi terrace deposits, and the question arises as to whether the dating has provided reliable finite ages. Tarapuhi terrace lies near the 'top' of the hill terrain near Haumuri Bluffs, and an age of ~100 ka necessitates there having been very rapid rates of erosion and landscape evolution since that time to produce the deeply incised landscape. We acknowledge that uplift rates may have varied over time, but if the ~0.75 mm/yr uplift rate of the ~80 ka Amuri Bluff terrace at Haumuri Bluffs is extrapolated back in time, there is a reasonable match of the ~95 m a.s.l. Kemps Hill paleoshoreline to MIS 5e (~120 ka) and the ~175 m a.s.l. Tarapuhi paleoshoreline to MIS 7 (~210 ka). This latter age seems more commensurate with the terrace position near the top of a highly dissected landscape. Further dating of the terraces at Haumuri Bluffs would be desirable to test the question of variable long-term uplift rates.

Section S3: Okarahia fluvial terraces

Fluvial terrace age constraints can be inferred from onshore/offshore gradient relationships (Merritts et al. 1994), taking account of the narrow continental shelf that reflects proximity of the Conway Trough submarine canyon and independently determined eustatic sea level chronologies (Siddall et al. 2003; Creveling et al. 2017), as shown conceptually in Figure S3.

The high terrace envelope has a steeper gradient than the coastal marine terraces and the modern Okarahia valley floor (Figure 7 of main text). The conceptual framework (Figure S3) thus implies that the high terrace envelope relates to low sea level and fluvial incision at the subaerially exposed head of the continental slope. A satisfactory fit is obtained with observed geomorphological features if the top of the high terrace landform set relates to the ~65 ka lowstand in MIS 3 (Figure 8B of main text), which would have maintained the shoreline at or below the shelf edge. We infer that the extreme lowstand of MIS 2 between ~30 and ~17 ka would have driven strong degradation of Okarahia Stream (Figure 8C of main text) forming a deeply incised channel out to the shelf edge. The inferred lowstand channel is not expressed in modern bathymetry, an understandable consequence of post-glacial sea rise whereby coastal erosion planed off the continental shelf and nearshore sedimentation filled in any low areas (Figure 8D of main text). A prominent indentation in Conway Trough's western flank (Figure 10 of main text; star) may mark a low-stand channel discharge point into the trough. A lack of other indentations in the trough flank along the Conway coast suggests that the Conway River's low-stand channel also discharged there.

Section S4: Structural modelling

Modelling of fault propagations folding was undertaken using FaultFold7, (http://www.geo.cornell.edu/geology/faculty/RWA/programs/faultfoldforward.html - last accessed April 2022) (Figure S4). These fault propagation folds were scaled to the Hundalee Fault. The models highlight that a planar fault will form a hanging-wall monocline, rather than an anticline. A hanging-wall anticline will only form if there is a change at depth in fault dip (Allmendinger 1998).

Section S5: Kaikōura Peninsula marine terraces and structural interpretation

A notable finding of the 2016 earthquake uplift mapping is that uplift was broadly uniform around the peninsula (Clark et al. 2017; Nicol et al. this issue), with similar uniformity in the uplift pattern represented in the pre-2016 uplifted Holocene beaches (Howell and Clark 2022). In contrast, a long-standing interpretation is that the Pleistocene marine terraces of Kaikōura Peninsula display a northwest tilt (e.g. Ota et al. 1996). However, Suggate's (1965; p. 61) description of the marine terraces provides a note of caution: "Viewed from the coast to the southwest, the Kaikoura Peninsula shows four distinct surfaces, the upper two apparently sloping gently westward, the lower two apparently horizontal." A ubiquitous assumption made for Kaikōura Peninsula by previous workers is that each Pleistocene terrace surface represents a paleo sea level datum, and that any current departure from horizontal represents post-formation tilt (e.g. Ota et al. 1996; Duffy 2020; Nicol et al. this issue). However, some of the Pleistocene terrace remnants extend more than 1 km from their associated paleo-cliff. Is it reasonable to assume that they represent a surface with no paleo relief?

We investigated this by preparing a geomorphic sketch map of the terrace surfaces and the bases of well-defined paleo sea cliffs (Figure S5a). In contrast to former areas of near-shore seabed, where paleo relief is a possibility and potentially difficult to quantify, the bases of paleo sea cliffs approximate a former shoreline and thus indicate an approximate paleo sea level (e.g. Duffy 2020). A proviso is that any coverbeds mantling the foot of the sea cliff introduce uncertainty as to the elevation of the shoreline (e.g. Duffy 2020). We mapped just those sections of former sea cliff where the cliff is prominently expressed in the landscape, but not areas where the presence of a former shoreline could be interpreted from relatively subdued changes in slope angle.

We found that across the entire peninsula, the bases of the prominent paleo sea cliffs occur at approximately 3 levels (neglecting the Holocene paleo sea cliff) relative to present sea level; ~80 m, ~60 m and ~45 m (Figures S5a and S5b). Also notable is the modern analogue of prominent sea cliffs and the inner shelf seabed around the northern, eastern and southern sides of Kaikōura Peninsula that extends to water depths of at least 20 m within ~1 km of the Holocene cliff-line (Figures S5a, S5b).

It would seem an exceptional circumstance if a sequence of marine terraces was tilted in such a way that the bases of a discontinuous set of prominent paleo sea cliffs happened to coincide with just three elevation levels. We think it more likely that paleo-bathymetric relief on some of the terrace surfaces has been mis-interpreted as tilt, and it is plausible that there is minimal tilt of the Pleistocene marine terraces. If correct, this would not affect the general uplift rate estimates derived from the Pleistocene terraces of the peninsula, (e.g. Duffy 2020; Nicol et al. this issue), but if no tilt needs to be accounted for, there may be no discrete late Quaternary offset on the inferred Armers Beach Fault (Nicol et al. this issue; Figure S5a). Our interpretation implies the estimated 23$\pm$5 m throw on the inferred fault (Nicol et al. this issue) represents paleo water depth of the order of 20 m some ~100-200 m seaward of the paleo cliff. Similarly steep seafloor gradients exist today immediately seaward of parts of the Holocene coastal platform along the southeast side of Kaikōura Peninsula (see Figure S5a). If the

Pleistocene terraces are not significantly tilted, there may be better accord between the Pleistocene and Holocene uplift pattern than has been suggested (Nicol et al. this issue).

Our wider structural interpretation of the Kaikōura Peninsula area is illustrated in Figure S5c. Due to the issues described above, we do not include the Armers Beach Fault. However, the 2016 uplift transition used to define a monoclinal flexure attributed to a buried fault, identified as the Te Taumanu Fault (Nicol et al. this issue), approximately coincides with the western margin of topographic relief associated with Kaikōura Peninsula. We link it to a suggested change in dip of our inferred Kaikōura Peninsula Fault (Figure S5c). The trend of the Te Taumanu surface monocline (Figure S6), as mapped by Nicol et al. (this issue) is ~035°, closer to the average strike of our inferred Kaikōura Peninsula Fault (~030°) than the ~045°-striking OSTF (Figure S6).

Section S6: Aftershock distributions

The hypothesised kinematics of the 2016 Kaikōura Earthquake are illustrated in relation to aftershock distributions, using the catalogue of relocated earthquakes of Chamberlain et al. (2021). We use that part of the catalogue representing aftershocks of the Kaikōura Earthquake, spanning from 14 November 2016 to 01 January 2020, plotted on the same base map used in Figure 12 of the main text. Figure 13 of the main text plots aftershocks equal or greater to magnitude 2.5, binned into 5 categories based on hypocentral depth. Figure S6 plots aftershocks equal or greater to magnitude 3.5, and for which a dominant sense of slip has been determined (three categories – normal, reverse or strike-slip). Each data point is plotted with the 5 depth categories applied in Figure 13, with the addition of a colour halo denoting slip sense.

References

Allmendinger RW. 1998. Inverse and forward numerical modeling of trishear fault-propagation folds. Tectonics. 17: 640-656. https://doi.org/10.1029/98TC01907.

Barnes PM, Audru J-C. 1999. Recognition of active strike-slip faulting from high-resolution marine seismic reflection profiles: Eastern Marlborough Fault System, New Zealand. Geological Society of America Bulletin. 111: 538–559.

Chamberlain CJ, Frank WB, Lanza F, Townend J, Warren-Smith E. 2021. Illuminating the pre-, co-, and post-seismic phases of the 2016 M7.8 Kaikōura earthquake with 10 years of seismicity. Journal of Geophysical Research: Solid Earth. 126(8):e2021JB022304. doi:10.1029/2021JB022304.

Clark KJ, Nissen EK, Howarth JD, Hamling IJ, Mountjoy JJ, Ries WF, Jones K, Goldstien S, Cochran U, Villamor P, et al. 2017. Highly variable coastal deformation in the 2016 MW7.8 Kaikōura earthquake reflects rupture complexity along a transpressional plate boundary. Earth and Planetary Science Letters. 474: 334-344.

Clement AJH, Whitehouse PL, Sloss CR. 2016. An examination of spatial variability in the timing and magnitude of Holocene relative sea-level changes in the New Zealand archipelago. Quaternary Science Reviews. 131: 73-101.

Creveling JR, Mitrovica JX, Clark PU, Waelbroeck C, Pico T. 2017. Predicted bounds on peak global mean sea level during marine isotope stages 5a and 5c. Quaternary Science Reviews. 163: 193-208.

Denton GH, Putnam AE, Russell JL, Barrell DJA, Schaefer JM, Kaplan MR, Strand PD. 2021. The Zealandia Switch: Ice age climate shifts viewed from Southern Hemisphere moraines. Quaternary Science Reviews. 257: 106771.

Duffy B. 2020. A geometric model to estimate slip rates from terrace rotation above an offshore, listric thrust fault, Kaikōura, New Zealand. Tectonophysics. 786: 228460.

Fleming CA, Suggate RP. 1964. The 550 ft raised beach at Amuri Bluff. New Zealand Journal of Geology and Geophysics. 7: 353-358.

Gibbard PL, Head MJ. 2020. The Quaternary Period. Geologic Time Scale 2020 (Volume 2). Pp. 1217-1255. https://doi.org/10.1016/B978-0-12-824360-2.00030-9.

Hogg AG, Heaton TJ, Hua Q, Palmer JG, Turney CSM, Southon J, Bayliss A, Blackwell PG, Boswijk G, Bronk Ramsey C, et al. 2020. SHCal20 Southern Hemisphere calibration, 0–55,000 years cal BP. Radiocarbon. 62: 759-778. doi:10.1017/RDC.2020.59.

Lewis DW, Ekdale AA. 1991. Lithofacies relationships in a late Quaternary gravel and loess fan delta complex, New Zealand. Palaeogeography, Palaeoclimatology, Palaeoecology. 81: 229-251.

Lisiecki LE, Raymo ME. 2005. A Pliocene-Pleistocene stack of 57 globally distributed benthic δ18O records. Paleoceanography. 20: PA1003. doi:10.1029/2004PA001071

Merritts DJ, Vincent KR, Wohl EE. 1994. Long river profiles, tectonism, and eustasy: A guide to interpreting fluvial terraces. Journal of Geophysical Research. 99 (B7): 14,031-14,050.

McConnico TS. 2012. The terraces of the Conway Coast, North Canterbury: Geomorphology, sedimentary facies and sequence stratigraphy. [PhD thesis]. University of Canterbury, 210 p.

McConnico TS, Bassett KN. 2007. Gravelly Gilbert-type fan delta on the Conway Coast, New Zealand: Foreset depositional processes and clast imbrications. Sedimentary Geology. 198: 147-166.

Nicol A, Begg J, Saltogianni V, Mouslopoulou V, Oncken O, Howell A. (this issue). Uplift and fault slip during the 2016 Kaikōura Earthquake and Late Quaternary, Kaikōura Peninsula, New Zealand, New Zealand Journal of Geology and Geophysics. DOI: 10.1080/00288306.2021.2021955

Oakley DOS, Kaufman DS, Gardner TW, Fisher DM, VanderLeest RA. 2017. Quaternary marine terrace chronology, North Canterbury, New Zealand, using amino acid racemization and infrared-stimulated luminescence. Quaternary Research. 87:151–167.

Oakley DOS, Fisher DM, Gardner TW, Stewart MK. 2018. Uplift rates of marine terraces as a constraint on fault-propagation fold kinematics: examples from the Hawkswood and Kate anticlines, North Canterbury, New Zealand. Tectonophysics.724–725:195–219.

Ota Y, Yoshikawa T, Iso N, Okada A, Yonekura N. 1984. Marine terraces of the Conway coast, South Island, New Zealand. New Zealand Journal of Geology and Geophysics. 27:313-325

Ota Y, Pillans B, Berryman KR, Beu AG, Fujimori T, Miyauchi T, Berger G, Climo FM. 1996. Pleistocene coastal terraces of Kaikoura Peninsula and the Marlborough coast, South Island, New Zealand. New Zealand Journal of Geology and Geophysics. 39:51-73.

Rattenbury MS, Townsend DB, Johnston MR. 2006. Geology of the Kaikoura area. Institute of Geological & Nuclear Sciences 1:250,000 Geological Map 13. 70 p. and map (1 sheet). Lower Hutt (NZ): GNS Science.

Seebeck H, Van Dissen RJ, Litchfield NJ, Barnes PM, Nicol A, Langridge RM, Barrell DJA, Villamor P, Ellis SM, Rattenbury MS, et al. 2022. New Zealand Community Fault Model – version 1.0. Lower Hutt (NZ); GNS Science. GNS Science Report 2021/57. doi:10.21420/GA7S-BS61.

Siddall M, Rohling EJ, Almogi-Labin A, Hemleben C, Meischner D, Schmelzer I, Smeed DA. 2003. Sea-level fluctuations during the last glacial cycle. Nature. 423:853-858.

Suggate RP. 1965. Late Pleistocene geology of the northern part of the South Island, New Zealand. Wellington: Government Printer. New Zealand Geological Survey Bulletin. 77. 91 p.

Warren G. 1995. Geology of the Parnassus area: Sheets O32 & part N32, Scale 1: 50 000. Institute of Geological & Nuclear Sciences Geological Map 18. 36 p. and map (1 sheet). Lower Hutt (NZ); GNS Science.

Williams CA, Eberhart-Phillips D, Bannister S, Barker DHN, Henrys S, Reyners M, Sutherland R. 2013. Revised interface geometry for the Hikurangi Subduction Zone, New Zealand. Seismological Research Letters. 84:1066–1073.

Table S1. Conway Flat radiocarbon samples described by Ota et al. (1984), with corresponding calendar ages (Hogg et al. 2020), and estimated sea level at the median age of the sample (after Clement et al. 2016).

Field ID[1]	Lab ID[1]	Sampled material [1]	Sample elevation (m a.s.l.) [1]	^{14}C age (^{14}C y BP)[1]	^{14}C error (± y)[1]	Calendar age (y BP, younger bound)[2]	Calendar age (y BP, older bound) [2]	Median calendar age (y BP) and uncertainty (± y) [2]	Estimated eustatic relative sea level at median age (m a.s.l.) [3]
A-1	N-3266	Wood at base of fluvial channel	7	3050	85	2955	3392	3174 ± 219	0 to +2
A-2	N-3267	Wood in silt	5	7350	105	7942	8348	8145 ± 203	-1 to -3
A-3	N-3268	Wood from tree in growth position	2	7670	90	8204	8597	8401 ± 197	-2 to -5
A-4	N-3269	Wood adjacent to tree stump	1	7730	120	8195	8974	8585 ± 390	-2 to -5
B-1	GaK-7923	Wood at base of fluvial channel	10	3550	110	3487	4088	3788 ± 301	0 to +2
B-2	GaK-7924	Wood adjacent to tree stump	2	8300	200	8600	9592	9096 ± 496	-7 to -9
B-3	GaK-7925	Wood from tree in growth position	2	8400	170	8778	9710	9244 ± 466	-7 to -10
577 [4]	NZ-533	Wood in gravel	2	7360	110	7945	8364	8155 ± 210	-1 to -3
578 [4]	NZ-546	Wood from tree in growth position	2	7750	90	8342	8764	8553 ± 211	-2 to -5

Notes:

[1] Based on information given in Ota et al. (1984), where details of samples 577 and 578 (NZ-533, NZ-546) are attributed to R.P. Suggate (pers. commun.)

[2] Calibrated using SHCal20, accessed at http://calib.org/calib/ (version 8.2). Bounds at 95% confidence (2 sigma), with arithmetically-calculated median age.

[3] From graphs of glacial-isostatic adjustment estimates for the New Zealand region in Clement et al. (2016).

[4] Equates to NZ Fossil Record file localities O32/f8577 and O32/f8578 (https://fred.org.nz/fred/index.jsp).

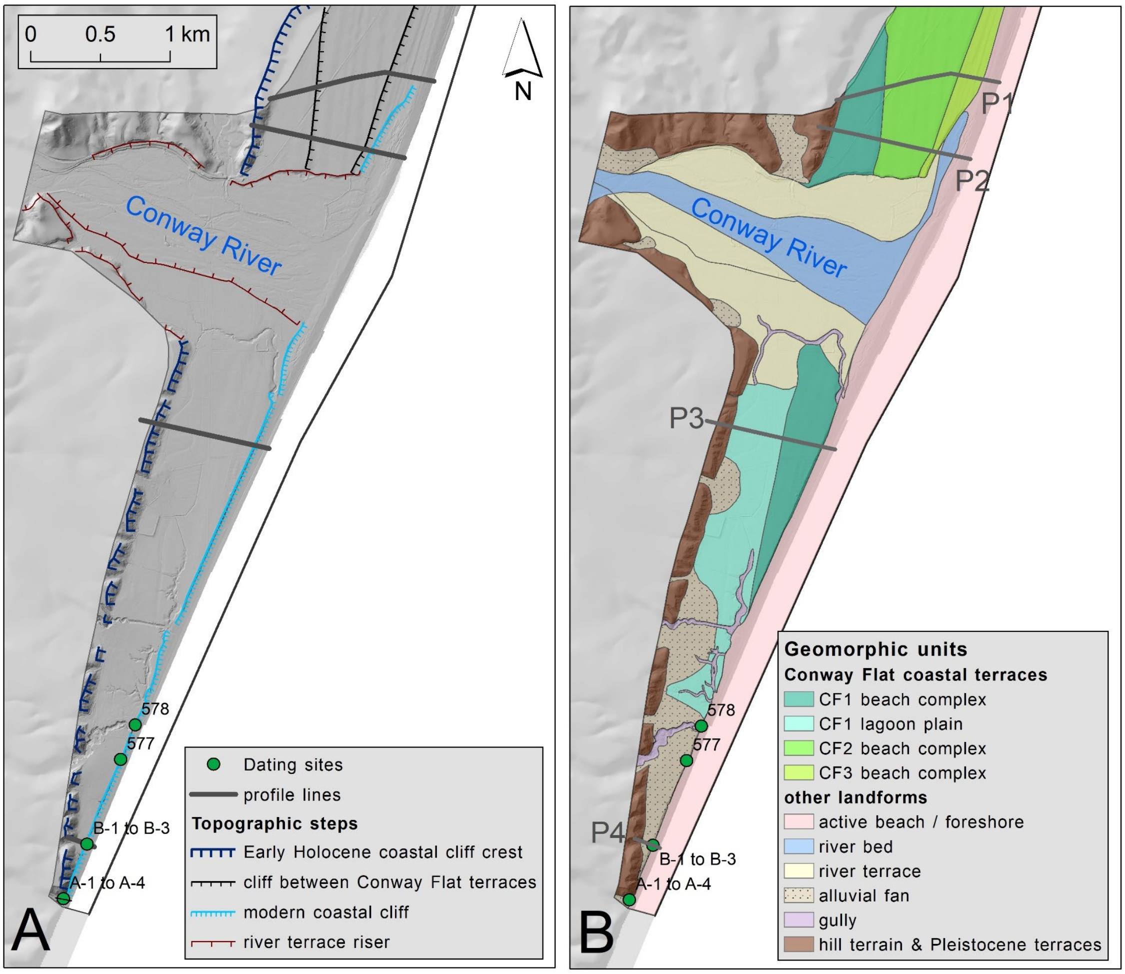

Figure S1. Geomorphological interpretation of part of the Conway Flat area (location in Figure 1 of main text). Panel A shows extent of 2016 lidar coverage as high-resolution DEM (darker grey) superimposed on a lower-resolution DEM (lighter grey), with notable topographic steps, radiocarbon dating after Ota et al. (1984) (see Table S1) and topographic profile lines generated from lidar. Panel B is at same scale and extent and includes an interpretive geomorphological map (after Ota et al. 1984). Profiles (P1-P4) are presented in Figure S2.

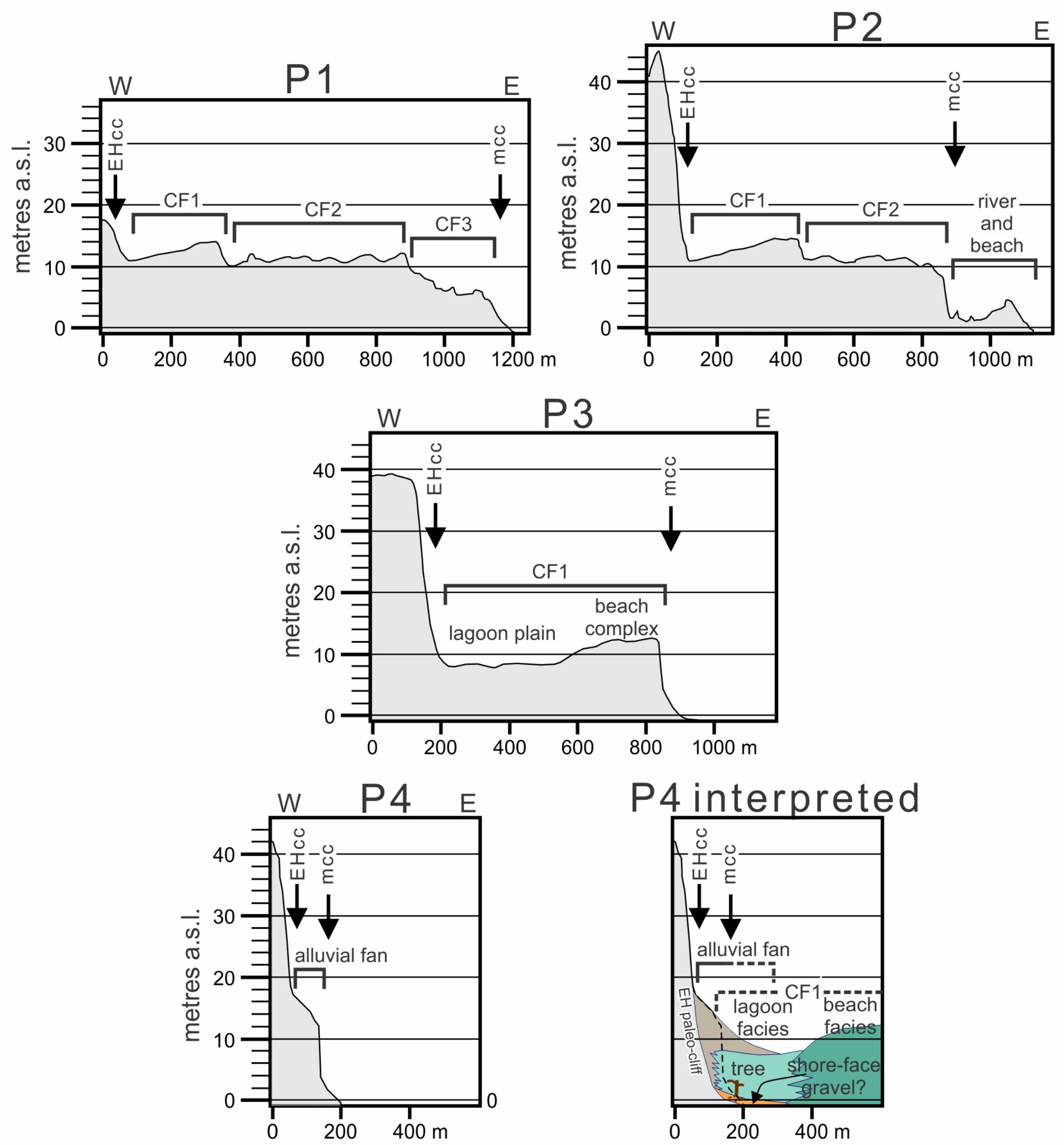

Figure S2. Topographic profiles across the Conway Flat terraces. Figure S1 shows location and geomorphic nomenclature. At lower right is a replicate of the P4 panel with a geological/geomorphological interpretation of the alluvial fan and CF1 lagoonal and beach deposits that are inferred to have been present, prior to their removal by modern coastal cliff retreat. Dashed horizontal lines illustrate inferred former extent of fan/terrace units. The interpretation highlights the relationship between the Early Holocene coastal cliff and the radiocarbon-dated (B-3) buried tree described from the modern coastal cliff exposure by Ota et al. (1984). EHcc = Early Holocene coastal cliff; mcc = modern coastal cliff; Conway Flat uplifted Holocene coastal terraces from oldest to youngest are CF1, CF2 and CF3.

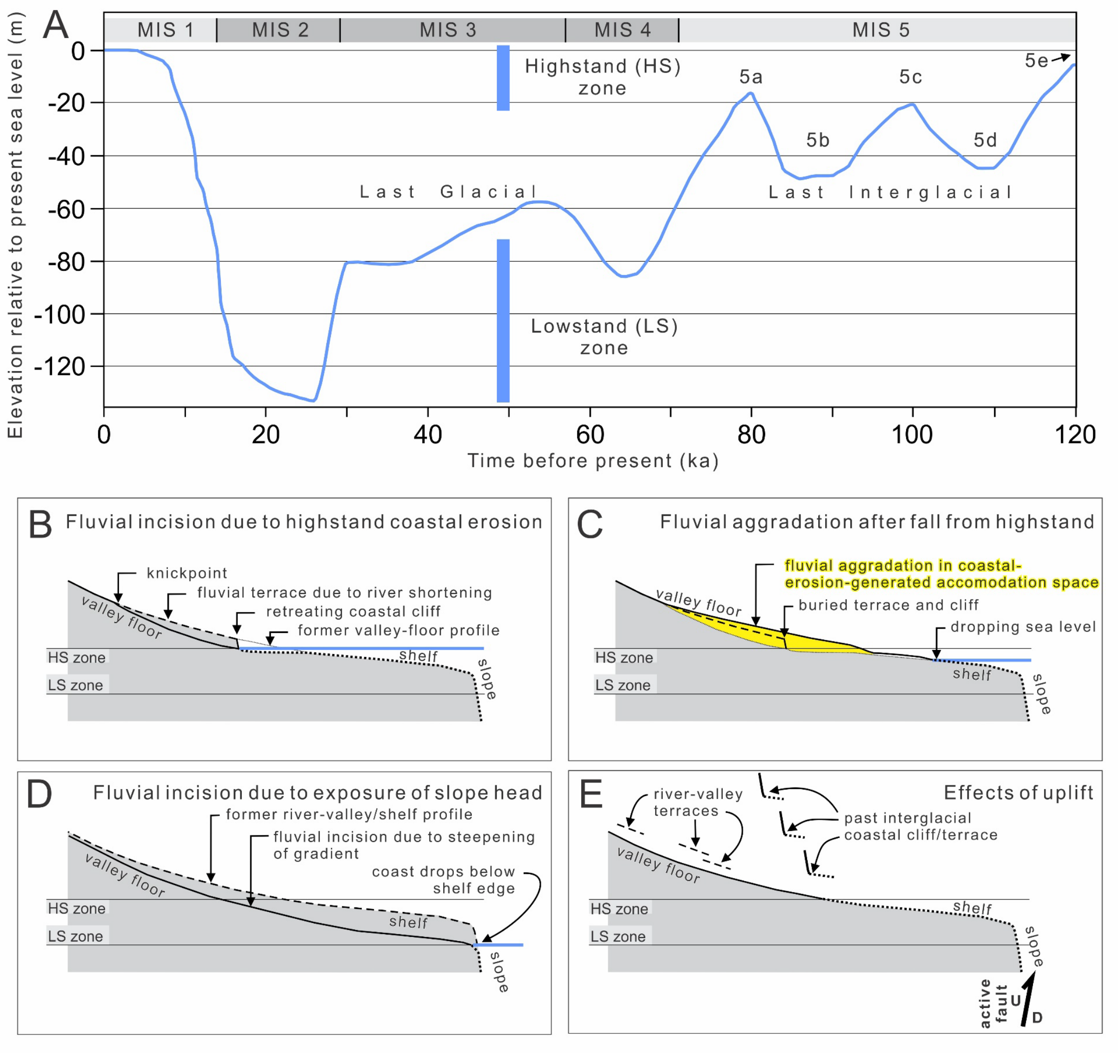

Figure S3. Influences of eustatic sea level change and uplift on terrace formation adjacent to the Conway coast. A: modelled eustatic sea level curve, taking account of glacio-isostatic adjustments, from Creveling et al. (2017). The ~3-km-wide continental shelf of the Conway coast, unusually narrow for New Zealand, creates notable demarcation between a 'highstand' (HS) zone of past sea levels, when the coast would have been on the inner part of the shelf, and a 'lowstand' (LS) zone when the coast would have intersected the steep continental slope. B-E: Diagrammatic profiles, approximating the Okarahia valley profile in Figures 8 and 9 of main text, but not to scale, illustrate likely effects of different sea levels on the fluvial system (B-D) and the effects of uplift (E). Scenarios shown are the formation of interglacial highstand cliff and marine erosion platform couplets (B; e.g. Amuri Bluff terrace), fluvial aggradation during marine regression (C; e.g. Claverley terrace), and steepening of fluvial systems under lowstand conditions (D).

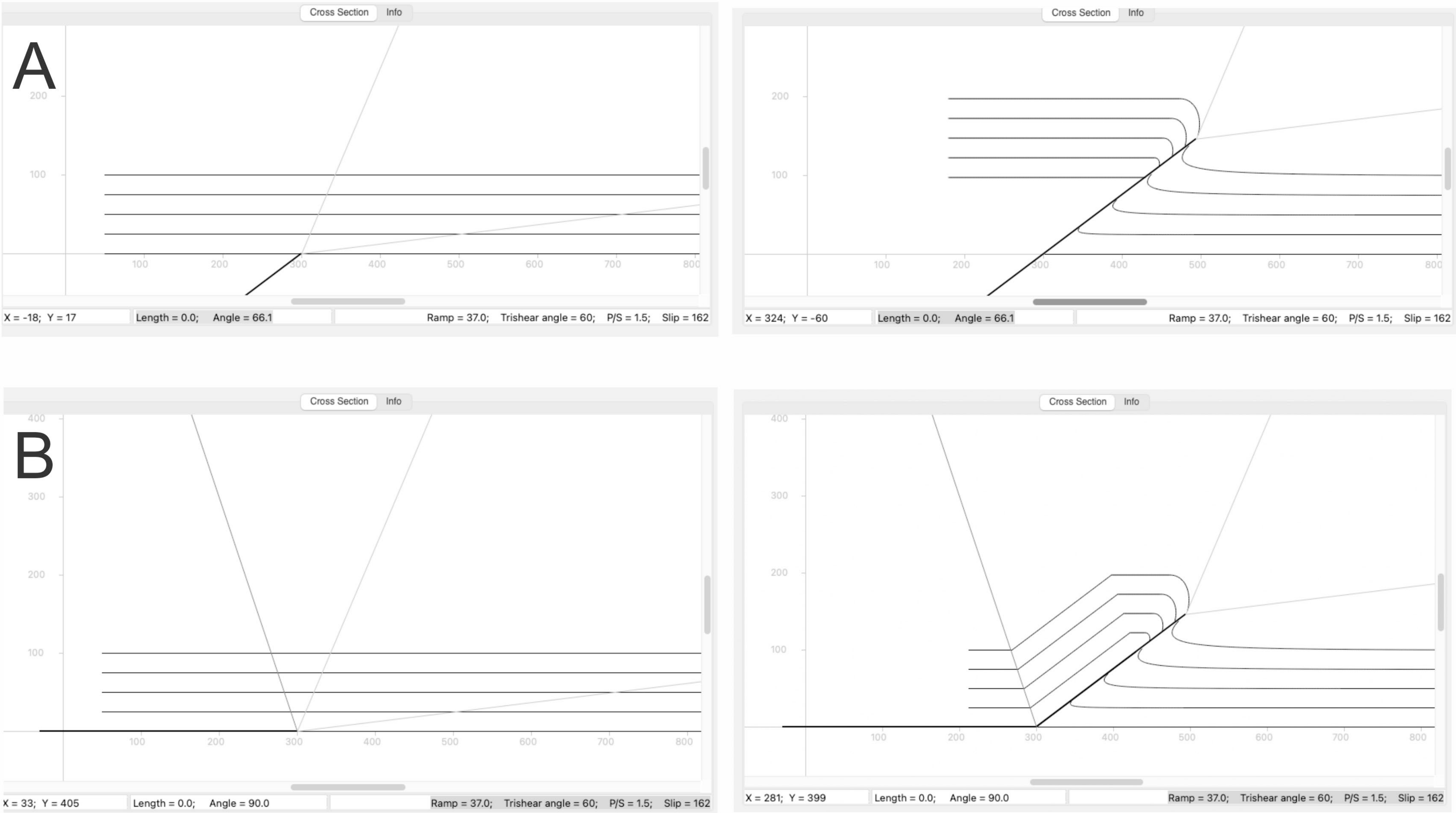

Figure S4. Fault propagation fold modelling, using software (FaultFold7) from https://www.rickallmendinger.net/faultfold (last accessed April 2022). A: The planar fault model produces a hanging wall monoclinal fold. B: The decollement fault and ramp model produces a hanging wall anticline.

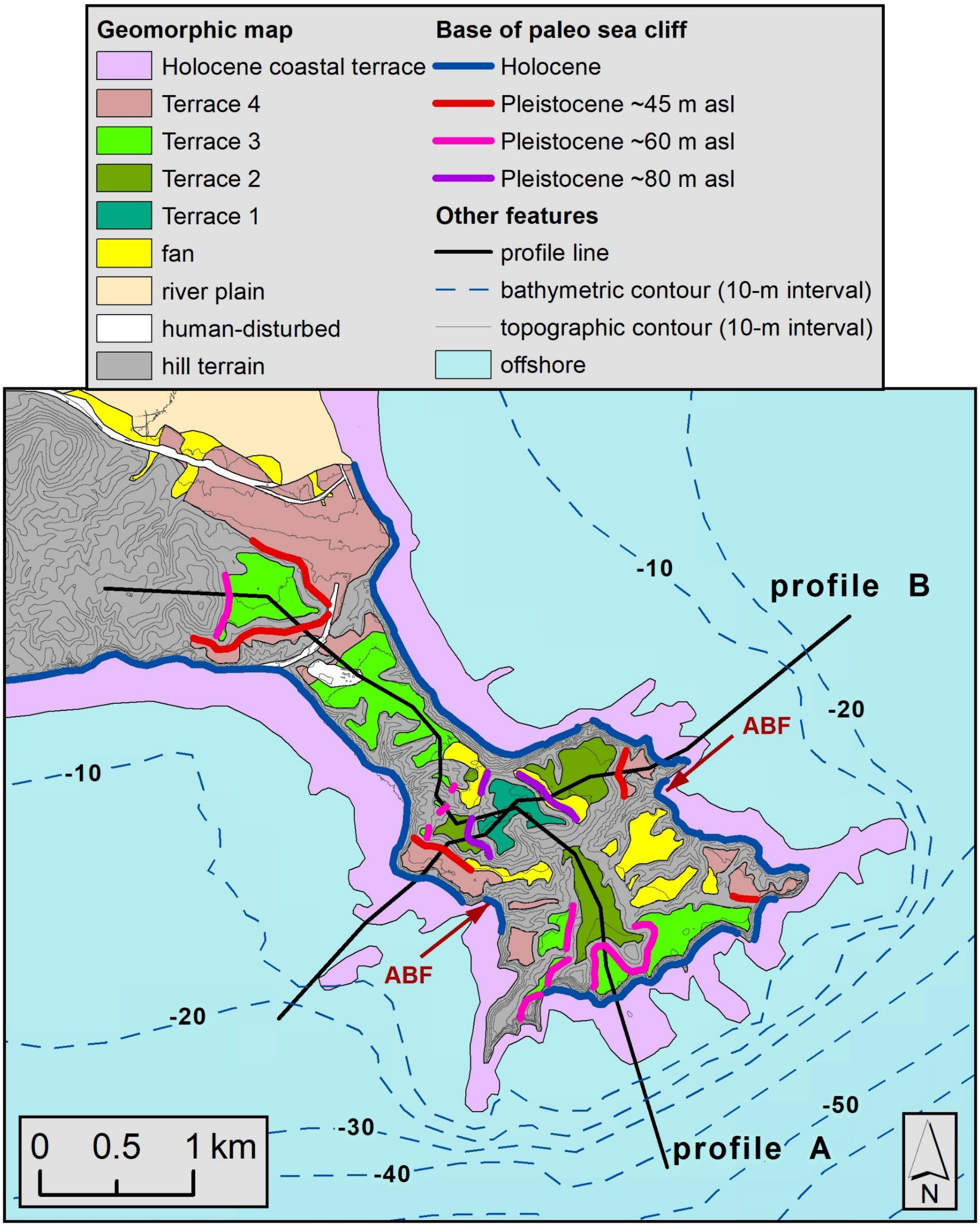

Figure S5a. Interpretive map of marine terrace surfaces on Kaikōura Peninsula. Pleistocene terraces numbered 1-4 from highest (oldest) to lowest (youngest). Lines denote the bases of prominent paleo sea cliffs, classified by approximate cliff-base altitude. See Figure S5b for profiles. Basemap is the post-2016 earthquake lidar hillshade model, with 10-m interval topographic contours generated from the lidar; bathymetric contours from the Rattenbury et al. (2006) geological map. Red arrows indicate the inferred Armers Beach Fault (ABF; Nicol et al. this issue).

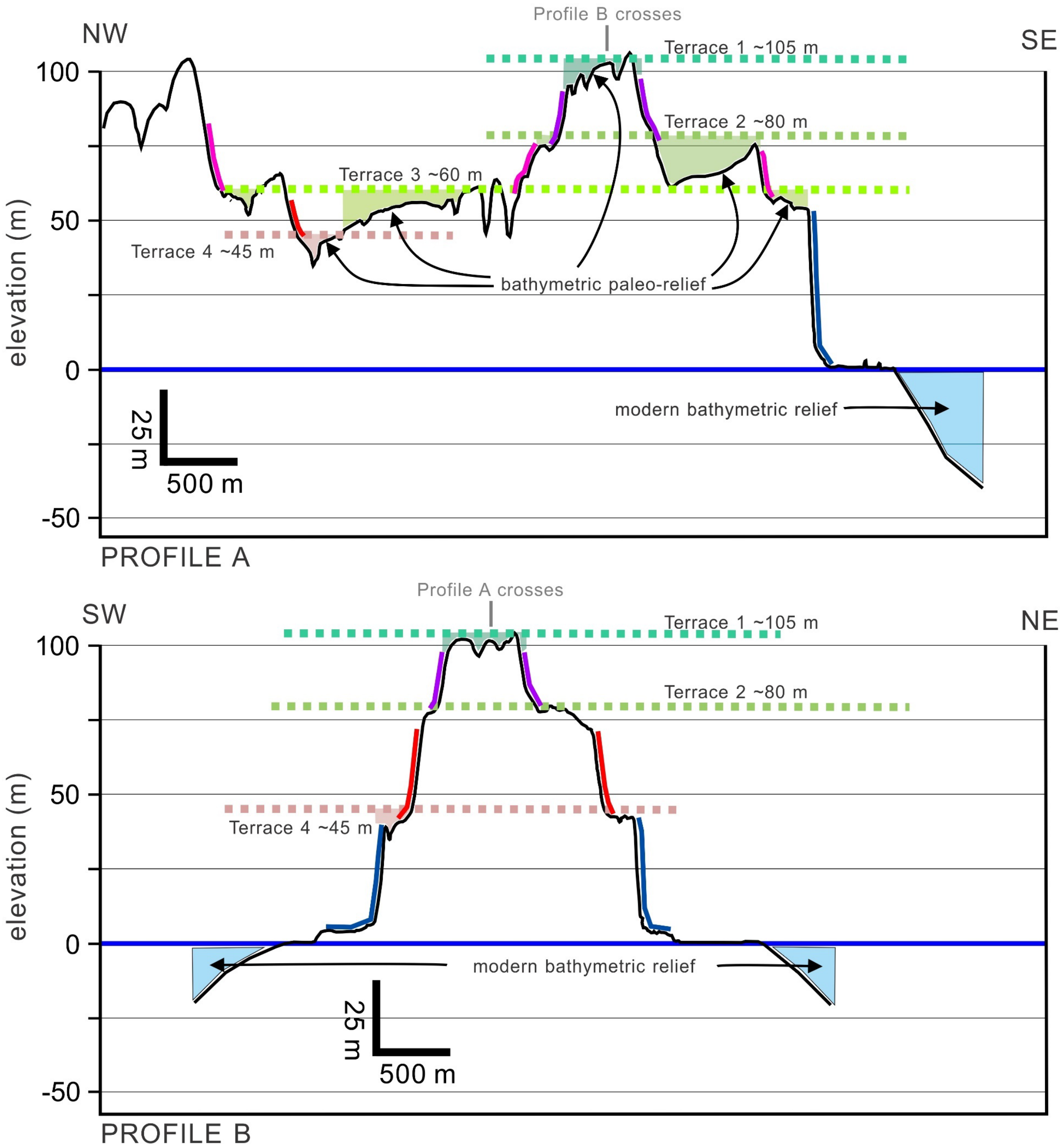

Figure S5b. Profiles A-B from Figure S5a. Black lines are land surface topography derived from the lidar dataset using the 3D Analyst tool in ArcGIS, and the modern bathymetry based on Figure S5a contours. Sectors of each mapped Pleistocene terrace surface interpreted to reflect paleo-bathymetry below the associated relative paleo-sea level are highlighted in colour shading. Paleo sea cliffs are illustrated using the colour scheme for cliff bases in Figure S5a.

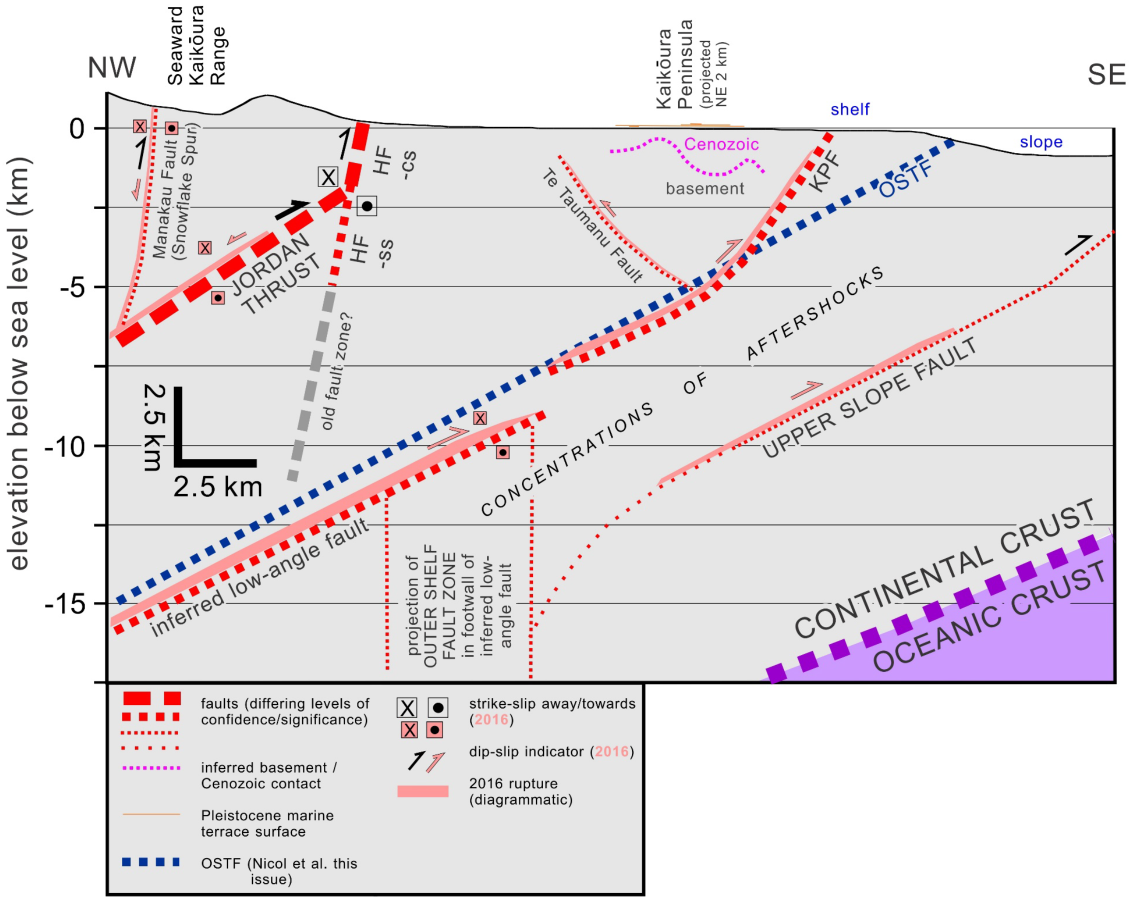

Figure S5c. Cross section immediately northeast of Kaikōura Peninsula (location in Figures 12 and 13 of main text, and Figure S6) illustrating structural elements of the hypothesised tectonic interpretation, in relation to the modelled Offshore Splay Thrust Fault (OSTF). See main text for discussion of interpretations. Geometry of main faults based on structure contouring (see Figure 12 main text). Hope Fault and Jordan Thrust dips from Seebeck et al. (2022). KPF = Kaikōura Peninsula Fault. Basement/Cenozoic contact based on Rattenbury et al. (2006). Outer Shelf Fault Zone projected along strike from mapping of Barnes and Audru (1999; see Figure 12 main text). Te Taumanu Fault after Nicol et al. (this issue). Pleistocene terrace profiles based on the interpretation in Figures S5a and b. Continental-oceanic crust contact based on Williams et al. (2013). Refer to Figures 13 and S6 for aftershock information. HF-cs = Hope Fault Conway segment; HF-ss = Hope Fault Seaward segment; KPF = Kaikōura Peninsula Fault. Non-connection between the low-angle fault and the KPF accords with how the Hundalee Fault is shown in Figure 12 (main text). See main text for more information.

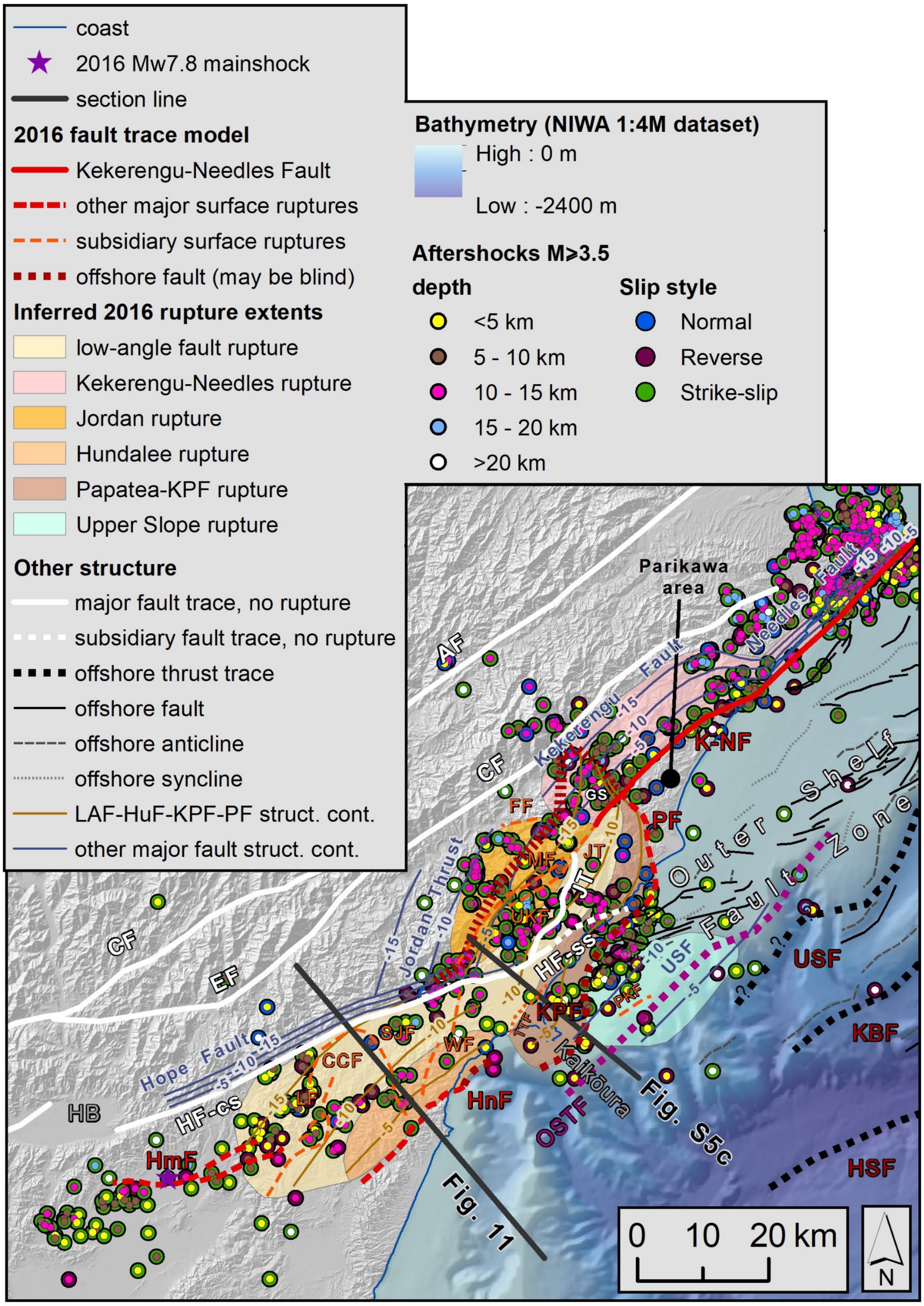

Figure S6. Hypothesised tectonic interpretation of the 2016 Kaikōura Earthquake (Figure 12 main text), showing aftershocks of magnitude ≥3.5, between 14 November 2016 and 01 January 2020 that have slip style attributes (from Chamberlain et al. (2021) dataset). Figure 12 (main text) gives abbreviations and other information. Orange dotted line northwest of Kaikōura is the monocline trace of the Te Taumanu Fault (TTF) from Nicol et al. (this issue). Aftershock symbol size in key is exaggerated for clarity.